High pressure electrical transport behavior in SrF_2 nanoplates*

Xiao-Yan Cui(崔晓岩)[1], Ting-Jing Hu(胡廷静)[1,†], Jing-Shu Wang(王婧姝)[1], Jun-Kai Zhang(张俊凯)[1], Xue-Fei Li(李雪飞)[1], Jing-Hai Yang(杨景海)[1], and Chun-Xiao Gao(高春晓)[2,‡]

[1] *Key Laboratory of Functional Materials Physics and Chemistry of the Ministry of Education, Jilin Normal University, Siping* 136000, *China*
[2] *State Key Laboratory of Superhard Materials, Jilin University, Changchun* 130012, *China*

(Received 19 December 2016; revised manuscript received 17 January 2017; published online 20 February 2017)

The charge transport behavior of strontium fluoride nanocrystals has been investigated by *in situ* impedance measurement up to 35 GPa. It was found that the parameters changed discontinuously at each phase transition. The charge carriers in SrF_2 nanocrystals include both F^- ions and electrons. In the *Fm*3*m* phase, pressure makes the electronic transport easier, while makes it more difficult in the *Pnma* phase. The defects at grain boundaries dominate the electronic transport process. Pressure could make the charge–discharge processes in the *Fm*3*m* phase much easier, but make it more difficult in the *Pnma* phase.

Keywords: electrical properties, phase transitions, transport properties

PACS: 64.60.–i, 72.20.–i, 07.35.+k **DOI:** 10.1088/1674-1056/26/4/046401

1. Introduction

Nanoscale materials have recently attracted considerable attention due to their special properties that are different from those of bulk materials.[1–4] In general, a decrease in crystal size implies an increased proportion of the surfaces (interfaces) and usually also in increased grain boundary (GB) properties. Therefore, the nanoscale material may have some unique transport properties that would not be presented in the bulk material, which is worth exploring.

The solid fluoride materials have been paid a great deal of attention due to their unique properties, such as low-energy phonons, high ionicity, electron–acceptor behavior, high resistivity, and anionic conductivity.[5–7] These properties lead to a wide range of potential applications in optics, biological labels, and lenses,[8,9] as well as components of insulators, gate dielectrics, wide-gap insulating overlayers, and buffer layers in semiconductor-on-insulator structures.[10] Alkaline earth metal fluorides have been extensively used as solid electrolytes to measure fluorine chemical potentials at high temperatures, and thus, to determine the Gibbs free energies of the formation of metal fluorides, oxides, carbides, and sulfides.[11,12] Their ambient and moderate temperature conductivities are relatively low.[13] This is a limitation of the use of alkaline earth metal fluorides as practical electrolytes for low temperature operations. In recent years, it was found that the F^- ionic conductivity in nanophase fluorides increases greatly in contrast to that in the corresponding coarse or single crystalline phase state.[14] As a result, with the development of nanometre materials, nanoscale alkaline earth metal fluorides are going to play an essential role in various applications based on their unique optical, electrical and magnetic properties. As an important kind of alkaline earth metal fluoride, strontium fluoride (SrF_2) has attracted a great deal of attention. At ambient conditions, the charge carriers of bulk SrF_2 are only F^- ions[12,13] and its conductivity is too small,[12,13] which limits the application of SrF_2 material. It is well known that both compression and decreasing crystal size treatments are effective methods for improving the material conductivity. However, there are few reports on the conductivity of SrF_2 nanocrystals under high pressures.

In this paper, we conducted an alternate-current (AC) impedance measurement of SrF_2 nanoplates at high pressures up to 35 GPa. The conduction mechanism involved in the charge transport process was studied.

2. Experimental section

In-situ impedance spectroscopy measurements of SrF_2 nanoplates were conducted at high pressure using a diamond anvil cell (DAC). The diamond culet face was 400 μm in diameter. A thin film of metal molybdenum was deposited on the surface of the cell by a magnetron sputtering system, and then patterned into a microcircuit with two sections by photoetching. Above the microcircuit, a film of aluminium oxide was sputtered to protect the microcircuit. The electrode ends were in exposure by removing the aluminium oxide chemically to make the probes contact the sample and connect to the electric

*Project supported by the National Natural Science Foundation of China (Grant Nos. 11374131, 11674404, 11404137, and 61378085), the Program for New Century Excellent Talents in University, China (Grant No. NCET-13-0824), the Program for the Development of Science and Technology of Jilin Province, China (Grant Nos. 201201079 and 20150204085GX), and the Twentieth Five-Year Program for Science and Technology of Education Department of Jilin Province, China (Grant No. 20150221).

†Corresponding author. E-mail: tjhumars@126.com
‡Corresponding author. E-mail: cc060109@qq.com

© 2017 Chinese Physical Society and IOP Publishing Ltd

meters. A detection window (120 μm×120 μm) was created in the center of the diamond culet. The distance between electrodes was 50 μm. The fabrication process of the microcircuit was reported previously.[15–18] The final microcircuit and the profile of our designed DAC are shown in Fig. 1.

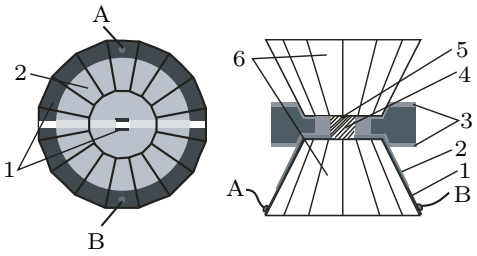


Fig. 1. (color online) Completed microcircuit on diamond anvil (left) and the profile of our designed DAC (right). Numbers marked on profile represent 1: Mo; 2: alumina layer; 3: insulating layer; 4: sample; 5: ruby; 6: diamond. A and B are the contact ends of the microcircuit.

A T301 stainless steel was pre-indented into 60 μm in thickness. Using the laser drilling machine, a hole of 250 μm in diameter was drilled at the centre of the indentation. Then, the insulating layer that mixed cubic boron nitride powder and epoxy was compressed into the indentation. Subsequently, a sample chamber of 150 μm was drilled. Pressure was calibrated by the R1 fluorescence peak of ruby. To avoid additional error on the electrical transport measurements, no pressure-transmitting medium was used. The impedance spectroscopy was measured by a Solartron 1260 impedance analyser equipped with a Solartron 1296 dielectric interface. A sine signal with amplitude of 1 V and frequency ranging from 0.1 Hz to 10^7 Hz were applied into the sample. The SrF_2 nanoplates were prepared by a liquid-solid-solution (LSS) solvothermal route. The sample is square with a mean dimension of (21±3) nm.[19]

3. Results and discussion

The Nyquist representation of the impedance spectroscopy of SrF_2 nanoplates under various pressures is shown in Fig. 2.

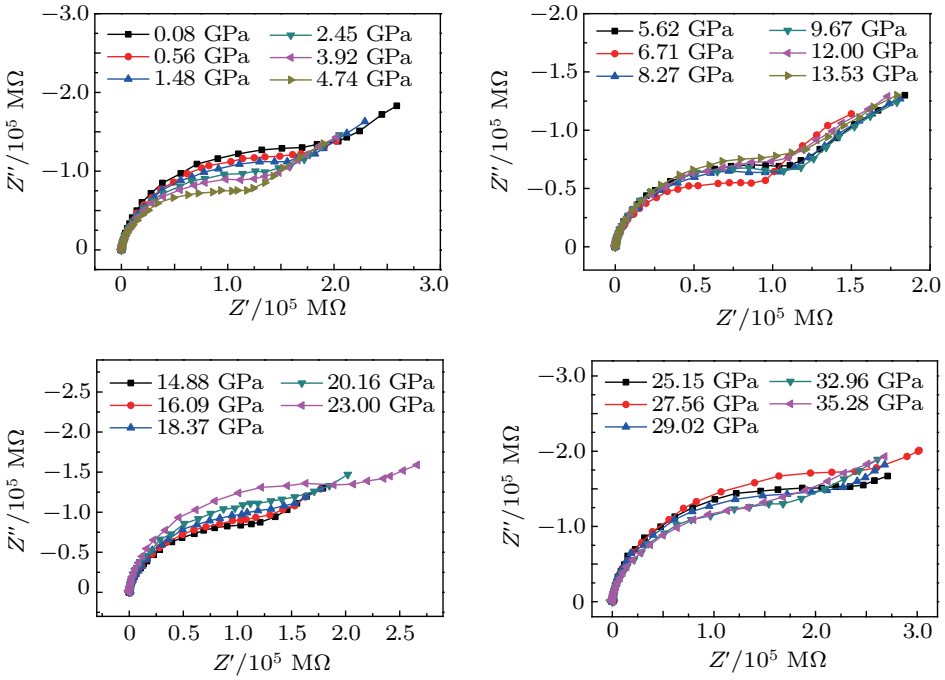


Fig. 2. (color online) Nyquist impedance spectra under various pressures.

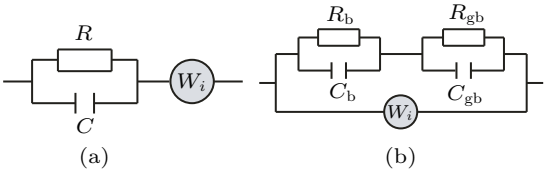


Fig. 3. (color online) (a) The equivalent circuit for only F^- ions conduction and (b) circuit diagram equivalent to the conduction mechanism. The subscripts b and gb of the *RC* parallel circuit represent bulk and grain boundary, respectively. W_i denotes the Warburg impedance.

As accepted for a solid sample, the equivalent circuit method is a reliable approach to describe the impedance spectra. To the bulk SrF_2, the charge carriers are F^- ions.[12,13] To the SrF_2 nanoplates, if the charge carriers are also only F^- ions, the equivalent circuit would be used as shown in Fig. 3(a), then the impedance spectroscopy would be shown as the hollow circle plot in Fig. 4. Therefore, the charge carriers in SrF_2 nanoplates include both ions and electrons. The equivalent circuit was used as shown in Fig. 3(b).

The agreement of the simulated spectra with the experimental data [Fig. 4] indicates the validity of considering both the ionic and electric conductions in SrF_2 nanoplates. The relaxation frequency of grains (f_b) can be obtained from the relationship of imaginary part Z'' versus frequency. The bulk resistance, grain boundary resistance, and grain relaxation frequency are shown in Fig. 5.

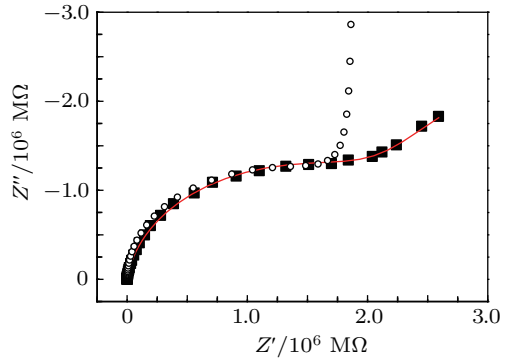


Fig. 4. (color online) Nyquist diagram at 0.08 GPa. The solid square represents the experimental result. The circle represents the result with only F^- ions conduction. The continuous line represents the simulated spectrum.

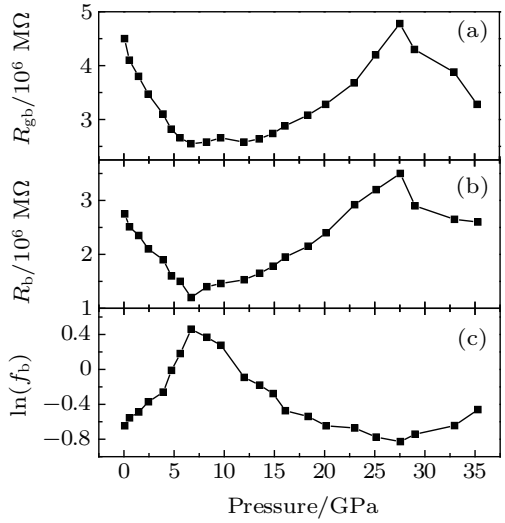


Fig. 5. Relationships of grain resistance, grain boundary resistance and grain relaxation frequency versus pressure.

From Fig. 5, it can be seen that each parameter changes discontinuously at about 6.71 GPa and 27.56 GPa. Because SrF_2 nanoplates undergo two phase transformations from $Fm3m$ to *Pnma* structure at 6.3 GPa, and then to $P6_3/mmc$ structure at 27.7 GPa,[19] the discontinuous changes can be attributed qualitatively to the pressure-induced structural phase transition. These results show that the phase transition is accompanied by the detectable changes in the electrical transport behavior.

In the $Fm3m$ phase, the grain interior and grain boundary resistance decrease with increasing pressure, while increase in the *Pnma* phase. This indicates that the grain and grain boundary microstructure are rearranged after the structural phase transition. In the $Fm3m$ phase, the pressure makes the electronic transport easier. In the *Pnma* phase, on the contrary, the pressure makes the electronic transport more difficult. In the whole pressure range, the grain boundary resistance shows a relatively larger contribution to the total resistance, which indicates that the defects at grain boundaries dominate the electronic transport process.

Puin *et al.* measured the conductivity of nanocrystalline CaF_2 at temperatures from 390 K to 500 K and found that the charge carriers are only F^- ions,[14] which is different from our results. The difference may be caused by the following reasons. (i) The sample preparation mothed: Puin *et al.* used the inert gas condensation method; we used the liquid–solid–solution (LSS) solvothermal route, which lead to the difference of the sample microstructure. (ii) The measurement conditions: Puin *et al.* conducted the measurement at temperatures from 390 K to 500 K, we conducted the measurement at room temperature, the temperature has different effects on the concentration and mobility of electron and ion, which finally leads to the difference of the charge carrier type.

The electron carrier transport in SrF_2 nanoplates grains can be regarded as a charging process in an *RC* resonance circuit and the relaxation frequency actually denotes the charge–discharge rate of the dipoles oscillation process, and its activation energy represents the energy to activate the resonance. The pressure dependence of activation energy can be obtained by fitting the pressure dependence of the bulk relaxation frequency in Fig. 5(c) to the differential form of the Arrhenius equation,

$$\mathrm{d}(\ln f_\mathrm{b})/\mathrm{d}P = -(1/k_\mathrm{B}T)(\mathrm{d}H/\mathrm{d}P),$$

where H represents the activation energy, k_B is the Boltzmann constant, and T represents room temperature. The results are listed in Table 1.

It can be seen that the activation energy decreases with increasing pressure in the $Fm3m$ phase, but increases in the *Pnma* phase. This indicates that the pressure could make the charge–discharge processes in the $Fm3m$ phase much easier, but make it more difficult in the *Pnma* phase.

Table 1. Pressure dependence of grain activation energy.

Pressure region/GPa	$(\mathrm{d}H/\mathrm{d}P)$/(meV/GPa)
0.08∼6.71	–4.03
14.88∼27.56	0.99

4. Conclusions

The charge transport behavior of strontium fluoride nanoplates has been investigated by *in-situ* impedance measurement at pressures up to 35 GPa. Each parameter changes discontinuously at about 6.71 GPa and 27.56 GPa, corresponding to the phase transitions of SrF_2 nanoplates under high pressure. The charge carriers in SrF_2 nanocrystals include both F^- ions and electrons. In the $Fm3m$ phase, pressure makes the electronic transport easier, while making it more difficult in the *Pnma* phase. The defects at grain boundaries dominate the electronic transport process. Pressure could make the charge–discharge processes in the $Fm3m$ phase much easier, but make it more difficult in the *Pnma* phase.

References

[1] Sun S, Weiss S and Alivisatos A P 1998 *Science* **281** 2013

[2] Moser A, Takano K, Margulies D T, Albrecht M, Sonobe Y, Ikeda Y, Sun S and Fullerton E E 2002 *J. Phys. D: Appl. Phys.* **35** R157

[3] Ambashta R D, Yusuf S M, Mukadam M D, Singh S, Wattal P K and Bahadur D 2005 *J. Magn. Magn. Mater.* **293** 8

[4] Rudge S R, Kurtz T L, Vessely C R, Catterall L G and Williamson D L 2000 *Biomaterials* **21** 1411

[5] Feldmann C, Roming M and Trampert K 2006 *Small* **2** 1248

[6] Quan Z W, Yang D M, Yang P P, Zhang X M, Lian H Z, Liu X M and Lin J 2008 *Inorg. Chem.* **47** 9509

[7] Gao P, Xie Y and Li Z 2006 *Eur. J. Inorg. Chem.* **16** 3261

[8] Mao Y B, Zhang F and Wong S S 2006 *Adv. Mater.* **18** 1895

[9] Wang W S, Zhen L, Xu C Y, Chen J Z and Shao W Z 2009 *Appl. Mater. Interfaces* **1** 780

[10] Singh R, Sinha S, Chou P, Hsu N J and Radpour F 1989 *J. Appl. Phys.* **66** 6179

[11] Pratt J N 1990 *Metall. Trans.* **21A** 1223

[12] Chandra S 1981 *Superionic Solids. Principles and Application* (New York: Oxford) pp. 313–370

[13] Laskar A L and Chandra S 1989 *Superionic Solids and Solid Electrolytes* (New York: Academic Press) pp. 339–379

[14] Prin W and Heitjans P 1995 *Nanostruct. Mater.* **6** 885

[15] Hu T J, Cui X Y, Gao Y, Han Y H, Liu C L, Liu B, Liu H W, Ma Y Z and Gao C X 2010 *Rev. Sci. Instrum.* **81** 115101

[16] Cui X Y, Hu T J, Han Y H, Gao C X, Peng G, Liu C L, Wu B J, Wang Y, Liu B, Ren W B, Li Y, Su N N, Zou G T, Du F and Chen G 2010 *Chin. Phys. Lett.* **27** 036402

[17] Hu T J, Cui X Y, Li X F, Wang J S, Yang J H and Gao C X 2015 *Chin. Phys. Lett.* **32** 016402

[18] Hu T J, Cui X Y, Li X F, Wang J S, Lv X M, Wang L S, Yang J H and Gao C X 2015 *Chin. Phys. B* **24** 116401

[19] Wang J S, Zhu H Y, Ma C L, Wu X X, Zhang J, Li D M, Cong R D, Liu J and Cui Q L 2013 *J. Phys. Chem. C* **117** 615